Robust improvement of the asymmetric post-buckling behavior of a composite panel by perturbing fiber paths

Sander van den Broek[a,*], Sergio Minera[b], Eelco Jansen[c], Raimund Rolfes[a]

[a]*Leibniz University Hannover, Hannover, Germany*
[b]*National Composites Centre, Bristol, United Kingdom*
[c]*Hogeschool Rotterdam, Rotterdam, the Netherlands*

Abstract

The buckling behavior of structures is highly sensitive to imperfections from the geometry and material properties of an ideal structure. In this paper, an approach is presented in which the effects of spatially varying fiber misalignments in composite structures are assessed through random field analysis and are subsequently used to improve the structure while simultaneously making it more robust to fiber misalignments. Random fields representing fiber misalignments generate a distribution of limit-point buckling loads. The stochastic analysis results generate a pattern used to perturb the unidirectional fiber paths. Perturbations are applied over a range of allowable fiber deviations and scaling factors, with different deterministic results. Random fields perturb the improved designs' fiber paths to quantify their sensitivity to deviations from the prescribed fiber path. The approach is applied to a composite panel exhibiting asymmetric post-buckling behavior, i.e., having an unstable post-buckling branch and an (initially) stable branch. Results show that perturbations in the fiber path can nudge a structure into a more stable post-buckling path by promoting a post-buckling path using local changes in structural stiffness. The robustness of improved designs can also increase, making structures less susceptible to local fiber misalignments.

Keywords: Random field, Robust design, fiber misalignment, Buckling, Composites, Steered fiber path

1. Introduction

It has long been the habit of designers to design structures using idealized homogeneous material properties within a structure. Deviations of these assumptions are taken into consideration by using a safety factor. Material properties found in manufactured composite structures can vary spatially. Variations occur due to manufacturing processes and allowable tolerances and can affect the shape [1], thickness [2], void content [3], fiber alignment [4], and other material properties [5, 6].

Quantifying the effects of such local variations have on structures can be done using random fields [7, 8, 9, 10, 11, 12]. Random fields are continuous spatial fields generated in one, two, or three dimensions. Fields contain random values associated with coordinates on the field; the coordinates' values are correlated with each other using a predefined correlation function, allowing for continuous variations of parameters.

Varying parameters can also improve performance or generate different behavior. Buckling loads can be improved by tailoring the thickness [13], applying seeded geometric changes to geometry [14, 15, 16], or tailoring the fiber path. Composite structures with engineered fiber paths are also known as variable stiffness composites and enable more careful tailoring of stiffnesses and tailor the buckling and out of plane behavior of structures [17, 18, 19, 20]. Variable stiffness structures also allow for bistability, in which a stable equilibrium exists in multiple configurations utilizing a combination of pre-stress and varying stiffnesses [21].

Several manufacturing techniques are suited to manufacture variable stiffness composites. Automated fiber placement (AFP) is one such technology in which tows of fibers are placed following curved paths. Conventional AFP machines use a compaction head that is perpendicular to the tangential placement direction. Shear in tows, which results due to in-plane bending deformation, can not be compensated. As tow-width increases

*Corresponding author
Email addresses: S.vandenBroek@isd.uni-hannover.de (Sander van den Broek), Sergio.Minera@nccuk.com (Sergio Minera), E.L.Jansen@hr.nl (Eelco Jansen), R.Rolfes@isd.uni-hannover.de (Raimund Rolfes)

and bending radius decreases, fiber breakage or wrinkling can become more of an issue. A lack of shear variability causes the width of the tow to vary with the bending radius, leading to overlaps or gaps between tows [22]. Gaps can be filled in using 3D printing technologies [23], where fiber-reinforced matrix material is deposited on any gaps formed, though this is a tedious and time-consuming process for mass production. Continuous tow shearing alleviates these issues by allowing shear within tows and compensating for deformation during placement using a pinching device, making much tighter turning radii possible [24, 25].

Tolerances in the placement and curing process cause small changes in the fiber angle, resin richness, and other material parameters. Local variations in stiffness caused by these changes can adversely affect the deterministic result. The argument could be made that any optimum found should be resilient enough to be insensitive to common variations [26]. Variable stiffness composites make it possible to make structures less sensitive to imperfections [27].

Structures with asymmetric post-buckling behavior have a stable and an unstable branch, corresponding to the two alternative directions of the relevant buckling mode and initial geometric imperfection shape. Which equilibrium path dominates depends on the imperfections found in the structure, making the structure very sensitive to imperfections. Imperfections can consist of deviations from a nominal geometry or, to a lesser extent, parameters affecting stiffness.

Tailoring a structure to incorporate small changes in its original design can improve the buckling load by increasing stiffness locally. This paper presents an approach to find patterns in which to apply local changes to the fiber angle of composite structures. Local variations are applied to the structure using random fields, affecting its buckling load. Analyzing the influence of local variations on the buckling load of a structure can give a non-dimensional pattern of influence of a structural parameter. Previous work of the authors has improved the deterministic linear buckling load of isotropic structures by tailoring the local thickness and Young's modulus [28]. Developments presented in this paper include its application on a non-linear problem, fiber angles of composite structures, and robustness analyses.

Developments are demonstrated on a composite curved panel by varying fiber angles using its nominal geometry. Deviations from a nominal fiber path can be achieved using existing techniques used to fabricate variable-stiffness composites. Fiber misalignments are generated on the structure using geodesic random fields. Running a Monte Carlo analysis quantifies the likelihood of reaching a particular limit-point buckling load. Patterns of the perturbed fiber paths are generated by analyzing the effects of local fiber misalignments and finding the local correlation between these variations and the buckling load. Deterministic results are analyzed from perturbed designs, after which the effects of introducing random fiber angle changes indicate the sensitivity of a perturbed fiber path to imperfections introduced during manufacturing.

The remainder of this paper introduces the methods used in section 2, starting with the structural model in section 2.1. Random variations to the fiber angle are generated using random fields. The generation and mapping of random fields is discussed in section 2.2. Analyzing stochastic results can lead to a pattern in which fibers are perturbed. Applying this pattern to the fiber paths leads to a deterministic improvement discussed in section 2.3. The robustness of improved designs can be analyzed by applying random fiber misalignments, this is discussed in section 2.4. An example of a curved composite panel is described in section 3.1, with baseline mechanical results without variations applied are shown in section 3.2. Section 3.3 adds perturbations on top of the baseline structure, quantifying and analyzing the effects fiber misalignments can have. Deterministic improvements are discussed in section 3.4, after which random variations are applied to analyze the perturbed fiber paths' sensitivity in section 3.5. The overall conclusions are discussed in section 4.

2. Methods

2.1. Structural formulation

Results are generated by using a structural model based on a Unified Formulation, making use of Serendipity Lagrange shape functions [29]. Extensions to the unified formulation enable the analysis of geometric non-linearity and curved elements [30]. Non-linearity is taken into account using an arc-length based solver.

2.1.1. Basic formulation

The structural model is a non-linear three-dimensional model. It utilizes a displacement field using two different shape functions in the cross-sectional plane ($F(x, z)$) and axial direction ($N(y)$).

Starting with a displacement field, $\boldsymbol{u} = [u, v, w]^{\mathrm{T}}$, the Green-Lagrange stress tensor $\mathbf{E}$ can be defined as

$$E_{ij} = \frac{1}{2}\left(\boldsymbol{u}_{,i} \cdot \boldsymbol{g}_j + \boldsymbol{u}_{,j} \cdot \boldsymbol{g}_i + \boldsymbol{u}_{,i} \cdot \boldsymbol{u}_{,j}\right), \tag{1}$$

where commas denote derivatives and $\boldsymbol{g}_i$ denotes a unit vector on the i axis. Displacement field $\boldsymbol{u}$ is approximated within the Unified Formulation as

$$\boldsymbol{u}_{(\mathrm{e})}(x,y,z) = F(x,z)N(y)\boldsymbol{u}_i, \qquad \text{with} \qquad i = 1,\ldots,n, \tag{2}$$

where n are the degrees of freedom of the model. For quasi-static problems, the elastic equilibrium is

$$\delta W_{\mathrm{int}} = \delta W_{\mathrm{ext}} \tag{3}$$

where W_{ext} and W_{int} are the external work and internal energy. Noting that the internal energy of the structure can be calculated as the sum of internal energy of all the elements $W_{\mathrm{int}} = \sum_e W^{(\mathrm{e})}_{\mathrm{int}}$ the internal energy can be expressed using the stress and strain tensors

$$\delta W^{(\mathrm{e})}_{\mathrm{int}} = \int_{V_{(\mathrm{e})}} \delta\boldsymbol{E} \cdot \mathbf{S} dV \tag{4}$$

in which $\mathbf{S}$ is the second Piola stress tensor. For non-linear analyses, it is of interest to create tangential matrices. Changes in internal energy are expressed as [31, sec. 3.1.1]

$$\delta(\delta W^{(\mathrm{e})}_{\mathrm{int}}) = \int_{V_{(\mathrm{e})}} \delta\left(\delta\boldsymbol{E} \cdot \boldsymbol{S}\right) dV, \tag{5}$$

$$= \int_{V_{(\mathrm{e})}} \delta\boldsymbol{E} \cdot \delta\boldsymbol{S}\, dV + \int_{V_{(\mathrm{e})}} \delta(\delta\boldsymbol{E}) \cdot \boldsymbol{S}\, dV, \tag{6}$$

where V is the volume of an element. Rewriting these in terms of non-linear contributions of the tangential and geometric stiffness matrices results in [32]

$$\delta(\delta W^{(\mathrm{e})}_{\mathrm{int}}) = \delta\boldsymbol{u}_j^{\mathrm{T}} \boldsymbol{K}^{(\mathrm{e})}_{(\mathrm{O})ij} \boldsymbol{u}_i + \delta\boldsymbol{u}_j^{\mathrm{T}} \boldsymbol{K}^{(\mathrm{e})}_{(\mathrm{G})ij} \boldsymbol{u}_i. \tag{7}$$

Rewriting the tangential stiffness matrix using eq. (7) leads to

$$\boldsymbol{K}^{(\mathrm{e})}_{(\mathrm{T})ij} = \boldsymbol{K}^{(\mathrm{e})}_{(\mathrm{O})ij} + \boldsymbol{K}^{(\mathrm{e})}_{(\mathrm{G})ij}, \tag{8}$$

where $\boldsymbol{K}^{(\mathrm{e})}_{(\mathrm{O})ij}$ is the non-linear contribution and $\boldsymbol{K}^{(\mathrm{e})}_{(\mathrm{G})ij}$ the geometric stiffness matrix. Explicit forms of these matrices can be found in [33, 34].

2.1.2. Formulation for curved elements

Returning to the displacement field approximation of eq. (2), the model used in the presented research uses Serendipity Lagrange shape functions in the cross-section (F) and Lagrange shape functions in the axial (N) direction. These shape functions are used to approximate the displacement field of the structure. The cross-sectional shape function F has either 4, 8, 12, 17, 23, or 30 degrees of freedom, depending on the order chosen. Hierarchical elements with four nodes are used in the current implementation.

Unlike most finite element formulations, different shape functions are used for the displacement field and the geometry. Using this approach, it is possible to have a higher fidelity representation of the geometry without increasing the degrees of freedom of the structural problem. This additional shape function $N^{3D}(\alpha,\beta,\xi)$ is defined within $[-1,1]^3$. Shape functions are defined in brick (e.g., 8, 27, or 64 nodes) elements. The three shape functions N^{3D}, $F(x,z)$, and $N(y)$ come together in a Jacobian matrix consisting of the shape derivatives of the shape function. These can represent curvilinear basis vectors [33].

2.2. Assigning random material variations

Variations analyzed in this paper are generated and applied by combining several different techniques and methods. These techniques have been previously applied and discussed in [28]. Geodesic distances define the correlation between points on a random field. Computing and mapping geodesic distances add complexity to the generation of fields in curved structures. This section will discuss the methods used to generate the geodesic distance array, generate the field, and map it to the structure.

2.2.1. Geodesics

Geodesic distance refers to the distance between points as it would be on a (curved) surface. On the other hand, Euclidean distance calculates the distance between two coordinates in space as a straight line. Finding the geodesic distance can be done with a variety of approaches. The most straightforward approach for this problem would be to find the shortest path between two points using the connectivity of a mesh. Utilizing a forward front in all directions to iteratively find the shortest distance is the most simplistic approach and first discussed by Dijkstra [35]. Such an approach tends to overestimate the distance, as it follows the edges of elements, while the shortest distance usually crosses over the face of an element (usually a polyhedron).

Finding the actual shortest distance over a mesh is a classic field of research in computational geometry, with many approaches being proposed and extended on over the years [36]. The approach used within this paper is based on the idea first published by Varadhan [37] and recently extended by Crane et al. [38]. In this approach, heat is introduced at a point on a mesh for a time t. Applying heat at a point generates a vector field of the heat flux on the surface. Normalizing this vector field generates a vector field of the shortest distances from the

origin point, after which the geodesic distance is calculated by solving the Poisson heat equation. Crane has shown how this approach can be pre-factored, significantly reducing the computational time when distances between many points are required, as is the case for random fields.

Geodesic distances used to generate the field are computed on a surface within the 3D model. The surface used spans the mid-plane of the structure. Using a surface reduces the number of distances to points that have to be computed, reducing the computational effort of generating a distance array and the decomposition to generate random fields.

2.2.2. *Generating random fields*

Random fields are stochastically generated distributions of a parameter in n dimensional space. Fields generated within this work are generated on a 2D plane within 3D space. These random variables' values are not entirely unrelated to each other, and actual variations are usually related to their neighboring variations. Defining how close points are to each other is why the geodesic length of section 2.2.1 is used to relate points. There are many different techniques to generate random fields [39]. Many of these methods have assumptions in space or correlation function. The method used within this work is called Covariance Matrix Decomposition (CMD) and has the advantage of its relative ease in implementation and combining with geodesic length.

Correlation of two sets X and Y is defined mathematically as [40, ch. 10]

$$\rho_{X,Y} = \frac{\operatorname{cov}(X,Y)}{\sigma_X \sigma_Y} = \frac{\mathrm{E}[(X-\mu_X)(Y-\mu_Y)]}{\sigma_X \sigma_Y}, \tag{9}$$

where ρ is the correlation, cov the covariance operator, μ_i the mean of set i, σ_i the standard deviation of set i, and E the expectation operator, within random fields, these sets represent points in a field and how they relate to each other. The correlation varies between 1 and -1 and indicates the relationship between the two sets. It is useful for generating random fields to define functions, which define the correlation as a function of distance. The fields generated in this paper use the correlation function

$$\rho_{k,l} = e^{-\left(\frac{\Delta L}{L_c}\right)^2}, \tag{10}$$

in which L_c is called the correlation length, and ΔL the (geodesic) distance between points k and l. This correlation function is widely used in literature and produces smooth continuous fields, well suited for in-plane fiber-angle variations [41]. Correlation length defines a length scale at which the correlation function of eq. (10) deteriorates. Experimentally measured correlation functions are not available in published literature and are highly dependant on the geometry and manufacturing process used. Studies analyzing random-field generated fiber imperfections on variable stiffness composites generally utilize a correlation length defined scale of curvature [42, 41] or a set distance, generally shorter than the scale of the structure [43].

The CMD method uses discretized points in space and assigns a random value to that value [44]. The field must be discretized fine enough to represent the transition in variation amplitude. The necessary refinement was studied by Li & Kiureghian [45] and found to be between $\frac{L_c}{4}$ and $\frac{L_c}{2}$ for the correlation function of eq. (10).

The CMD method decomposes the correlation matrix. This decomposed matrix can be used to calculate random fields through simple multiplication with a random vector $\boldsymbol{\chi}$ with unit variance, and zero mean. The first step in generating fields is to build a correlation matrix of all points h_i of the field,

$$R_{ij} = \frac{\operatorname{cov}\left(h_i, h_j\right)}{\sigma_i \sigma_j} \rightarrow \tag{11}$$

$$\mathbf{R} = \begin{bmatrix} 1 & \rho\left(h_1,h_2\right) & \dots & \rho\left(h_1,h_n\right) \\ \rho\left(h_2,h_1\right) & 1 & \dots & \rho\left(h_2,h_n\right) \\ \vdots & & \ddots & \vdots \\ \rho\left(h_n,h_1\right) & \rho\left(h_n,h_2\right) & \dots & 1 \end{bmatrix}. \tag{12}$$

where $\rho(y_i, y_j) = \rho(y_j, y_i)$, noting that the correlation here can be calculated using eq. (10).

Taking the definition of covariance

$$\operatorname{cov}\left[X,Y\right] = \mathrm{E}\left[XY\right] - \mathrm{E}\left[X\right]\mathrm{E}\left[Y\right], \tag{13}$$

and keeping in mind the field has a mean of zero, it is possible to show that $\mathbf{R}$ can be decomposed into two matrices,

$$\begin{aligned} \mathbf{R} &= \operatorname{cov}[\boldsymbol{x},\boldsymbol{x}] = \mathrm{E}(\boldsymbol{x},\boldsymbol{x}^T) - 0 \cdot 0 \\ &= \mathrm{E}(\mathbf{L}\boldsymbol{\chi}(\mathbf{L}\boldsymbol{\chi})^T) = \mathbf{L}\mathrm{E}(\boldsymbol{\chi}\boldsymbol{\chi}^T)\mathbf{L}^T = \mathbf{L}\mathbf{I}\mathbf{L}^T = \mathbf{L}\mathbf{L}^T. \end{aligned} \tag{14}$$

From eqs. (10) and (11) the matrix $\mathbf{R}$ is symmetric and positive definite, the eigenvalues should all be positive and real. This decomposition is done by using eigendecomposition in the form of

$$\mathbf{R} = \mathbf{Q}\boldsymbol{\Lambda}\mathbf{Q} \tag{15}$$

in which $\mathbf{\Lambda}$ is a diagonal matrix with the eigenvalues of $\mathbf{R}$, and $\mathbf{Q}$ contains the eigenvectors of the matrix. Matrix $\mathbf{L}$ can be extracted from this as

$$\mathbf{R} = \mathbf{Q}\hat{\mathbf{\Lambda}}\hat{\mathbf{\Lambda}}\mathbf{Q} = \mathbf{L}\mathbf{L}^T \rightarrow \mathbf{L} = \mathbf{Q}\hat{\mathbf{\Lambda}}, \tag{16}$$

in which $\hat{\mathbf{\Lambda}} = \text{diag}(\sqrt{\lambda})$, λ being the eigenvalues of the $\mathbf{R}$ matrix. Using the decomposed correlation matrix $\mathbf{L}$, it is possible to generate random fields using

$$\mathbf{f} = \mathbf{L}\boldsymbol{\chi}. \tag{17}$$

Decomposing is only necessary once, after which random fields are generated with a minimal computational cost.

2.2.3. Mapping random fields to structure

Fields are generated on a 2D (surface) within a 3D structure, not having any variability through the thickness of the structure, which is considered negligible for thin-walled structures. 3D brick elements described in section 2.1.2 are used to map the field into a 3D space. Discretization of fields are not directly related and can be refined independently depending on their optima. Structures containing much curvature may benefit from a finely discretized random field (as the geodesic distances would be more accurate) while not necessarily needing a considerable refinement in structural elements to converge to accurate results.

While initializing, the analysis nodes of the geometric mesh are projected on the random field mesh. Random field element numbers and local coordinates are stored, creating a mapping between the two meshes. As this mapping is the same for all analyses, it only has to be done once and can be reused during the stochastic analysis. Values of the random field are evaluated using the shape function of the geometric mesh. Figure 1 shows how a point in the structure i has element coordinates within the geometric mesh α, β, ξ.

During assembly of the stiffness matrix, the material properties are assigned as

$$\theta_{pt} = \theta_\mu + f_{pt}\theta_\sigma \tag{18}$$

in which θ_{pt} is the material orientation at point $_{pt}$, θ_μ is the mean value of θ, f_{pt} is the value of the random field at the point and θ_σ is the standard deviation of material parameter θ.

2.3. Deterministic improvement

Deterministic improvement of the buckling load of the baseline structure is achieved by analyzing the effects of random variations applied to the fiber angle.

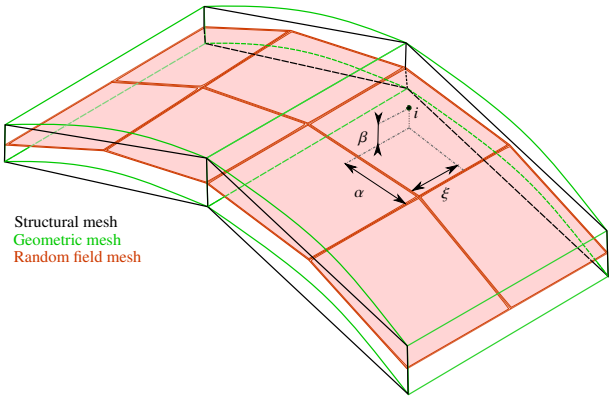

Figure 1: Discretizations found in the structure, and the coordinates of i as projected into the geometric mesh [28]. Coordinates are then used to evaluate the value of a random field in the volume of the element.

The authors' previous work has led to an increase of linear buckling loads by varying the thickness of Young's modulus in similar structures [28]. Similar to that approach, correlation patterns of fiber angle variations of every layer show the local influence of fiber angle changes. Improvement in the buckling load is achieved by scaling this correlation pattern, perturbing the fiber paths of the baseline design.

2.3.1. Generating correlation patterns

Independent random fields are generated for every layer of a structure. These random fields represent small angle variations of the fiber paths in each layer. Variations generated can be modeled to be similar to real fiber path deviations but can also be fictitious.

Extending eq. (9), it is possible to generate the local correlation pattern over n samples using

$$H_{i,j} = \frac{\sum_{k=1}^{n}\left(f_{lim,k} - \bar{f}_{lim}\right)\left(\theta_{i,j,k} - \bar{\theta}_i\right)}{\sqrt{\sum_{k=1}^{n}\left(f_{lim,k} - \bar{f}_{lim}\right)^2}\sqrt{\sum_{k=1}^{n}\left(\theta_{i,j,k} - \bar{\theta}_i\right)^2}} \tag{19}$$

where $H_{i,j}$ is the correlated value of the buckling load f_{lim}, and fiber angle variation at point i at layer j. Parameter $\theta_{i,j,k}$ is the fiber angle variation at point i, layer j, and sample k. Mean values of parameters are indicated using $\bar{\cdot}$.

The pattern generated infers the average influence a local fiber angle variation has on the buckling load. Applying this field to perturb the fiber path can thereby lead to an improvement in the buckling load of the structure. Patterns formed inherit the correlation of points to the distance defined by the correlation function of eq. (10). Correlation in the distance within random variations leads to a continuity in the correlation pattern and

defines its length scale. Correlation patterns generated using a large correlation length will vary over a relatively large distance. Shorter correlation lengths will lead to correlation patterns with more localized deviations, and a higher potential improvement [28]. Which correlation length to use while generating correlation patterns may also be determined by manufacturing considerations. As tighter fiber-placement curvatures are possible, the correlation length can become shorter.

2.3.2. Applying correlation pattern onto structure

Values of the correlation pattern show a non-dimensional relative influence of local variations. Applying these patterns to a structure first requires proper scaling. Normalization is first applied to the fields so that they fit in the range [-1,1]. Analyses within this paper utilize a normalization in which the global minima and maxima (over all fields) correspond to this range, not the individual layers minima and maxima.

Using this normalized field $\hat{\mathbf{H}}$ variations are computed using a maximum variation parameter ϕ, and a scaling parameter m. During matrix assembly, these parameters are used to evaluate material orientation using

$$\theta_{i,j} = \theta_{0,i,j} + \hat{H}^m_{i,j}\phi_{i,j}, \tag{20}$$

where $\theta_{0,i,j}$ is the original material orientation.

Optimal values of m and ϕ depend on the structure in question and the desired reliability if there are stochastic variations present of the parameter in the structure.

2.4. Robustness analysis

The approach described in section 2.3 can deterministically improve the structural performance by adding small variations in the material orientation (e.g., fiber angle). During manufacturing, random variations of material orientation can occur due to production processes. Robustness defines the effect that such imperfections have on the structure. When a design becomes more robust, the response becomes less sensitive to variations [46].

Improvements found using deterministic methods may be more sensitive to these random variations. These deterministic solutions are subjected to small local variations in fiber angle to analyze the robustness of the deterministic design with respect to fiber misalignments. Ideally, these would reflect real-world manufacturing tolerances, but even fictional variations can give a qualitative representation of the sensitivity of a structure to spatial fiber misalignments.

The fiber-alignment sensitivity of improved structures can be evaluated by comparing the statistical distribution of the buckling load of the baseline structure under random influences to that of the improved structure. Material orientation at every point i at layer j can be evaluated as

$$\theta_{i,j} = \underbrace{\theta_{0,i,j}}_{\text{Original}} + \underbrace{\hat{H}^m_{i,j}\phi_{i,j}}_{\text{Deterministic perturbation}} + \underbrace{\mathbf{f}_{i,j}\theta_\sigma}_{\text{Random variation}}, \tag{21}$$

where the deterministic perturbation $\hat{\mathbf{H}}$ equals zero for the baseline configuration.

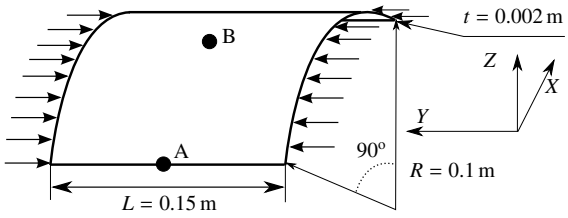

Figure 2: Curved panel geometry

Material properties			
E_1	142 GPa	$E_2 = E_3$	10.3 GPa
G_{23}	4.28 GPa	$G_{13} = G_{12}$	7.2 GPa
ν_{23}	0.4	$\nu_{13} = \nu_{12}$	0.27

Table 1: AS4 carbon fiber properties, taken from [47]

3. Numerical example

To demonstrate the approach discussed in section 2, the approach is applied to a composite curved panel similar to the one analyzed in [10]. Analyses of the baseline structure without any variations applied show the linear and non-linear behavior of a structure without any variations applied. Following these baseline results, stochastic variations are applied to the structure, providing information on the effects of variations on the buckling load of the structure. Effects of these stochastic runs are then processed to find a correlation pattern across the structure. Perturbations of the fiber paths are made on the structure to improve the buckling load. These deterministic solutions are finally evaluated to quantify their ability to withstand spatial fiber misalignments.

3.1. Structure and solver

Dimensions of the panel are shown in fig. 2. Three layers of anisotropic material are applied in a [90°,0°,90°] configuration, where 0° aligns with the y-axis. Table 1 lists the material properties of the layers.

The discretization of the structure consists of 10x3 third-order Serendipity Lagrange elements in the cross-section and ten elements in the axial direction. The

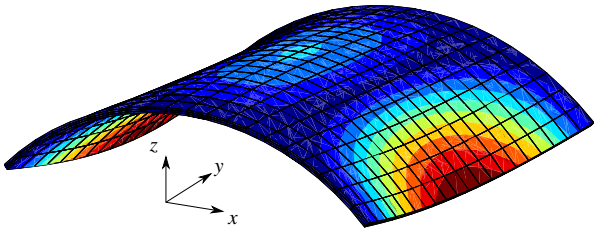

(a) Displacement shape of stable branch I of fig. 5

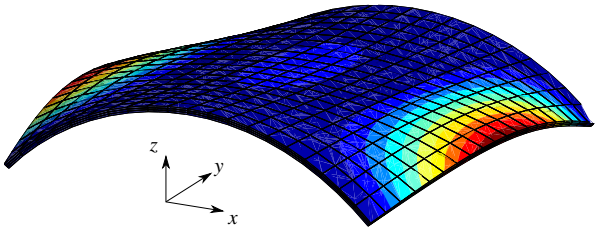

(b) Displacement shape of initially unstable branch II of fig. 5

Figure 3: Scaled deformation shapes of the curved panel at buckling load

structure has a total of 17 670 degrees of freedom over all these elements.

Boundary conditions and loads consist of distributed loads applied on the edges of $y = 0$ and $y = 0.15$ totaling 1 N. Constraints limit out of plane displacement on the loaded edges. Axial displacement is constrained using two points on one of the loaded edges in the axial (y) direction.

Variations of the material orientation/fiber angle are applied of $\theta_\sigma = 2°$. Fiber deviations, studied by Yurgartis, showed a measured range of up to this value [4]. Fields generated in this study use a correlation length of 25 mm for both correlation pattern generation and robustness analyses.

Analyses done in the following sections all utilize a non-linear solver. Buckling loads of the configurations are determined by using an arc-length based solver. Load is slowly increased until it deceases 5 sequential steps, the (limit-point) buckling load is the highest load found in the analysis.

3.2. Baseline analysis

Baseline results of the structure reach a buckling load of 22.1 kN. Deformations are in the form shown in fig. 3b. Curved panels have asymmetric bifurcation behavior with an initially stable, as well as unstable equilibrium. Deformations indicate that the baseline solution follows the unstable branch of the asymmetric bifurcation.

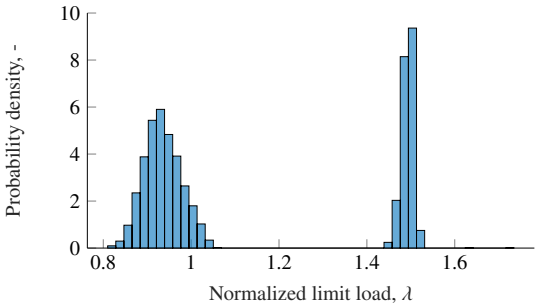

Figure 4: Probability density plot of the buckling load of the baseline structure subjected to 2° variations of fiber angles, normalized to the baseline load

3.3. Stochastic analysis

Effects of fiber variations are analyzed by applying independent random fields to the three layers' fiber angles. Samples with random fields are generated and run 5000 times, generating the probability density shown in fig. 4.

Displacements in the z-direction show distinct branching in responses. Figure 5 shows displacement results of all the stochastic runs, highlighting four representative responses showing the different load-displacement paths. Branches I and II both have two mirrored versions of each other, depending on which side of the structure forms the buckle. Scaled initial post-buckling displacements corresponding to these paths are shown in figure fig. 6.

Both of the equilibrium paths generate distinctly different responses. Lower load levels between 0.8-1.05 belong to the unstable branch II shown in fig. 3b, the initially stable branch I of fig. 3a has a buckling load thats approximately 50% higher.

Analyzing the two equilibrium paths, 62% of samples follow the unstable branch II, and 38% follow the initially stable branch I. Due to these two branches distinctly different characteristics, both branches are analyzed separately.

The unstable branch II, with λ between 0.8-1.1 has a mean value of 20.67 kN (0.935 λ) with a standard deviation of 934 N (0.042 λ), corresponding to a coefficient of variation of 4.52%. Branch II with initial stable behavior has a normalized buckling load around λ= 1.5, equaling a mean value of 32.99 kN (1.494 λ), with a standard deviation of 322 N (0.0147 λ) equalling a coefficient of variation of 0.975%.

3.4. Deterministic improvement

Improving the design is done by analyzing the runs done in section 3.3, finding the correlation between lo-

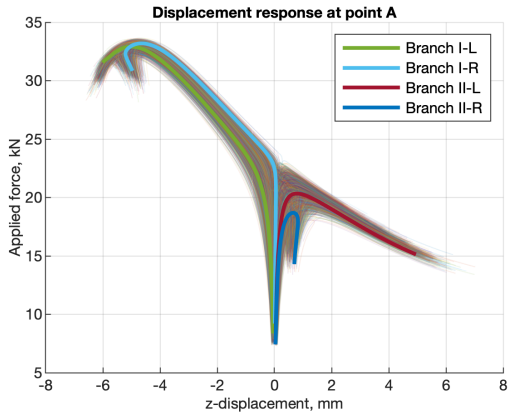

(a) Results of z-displacements at point A

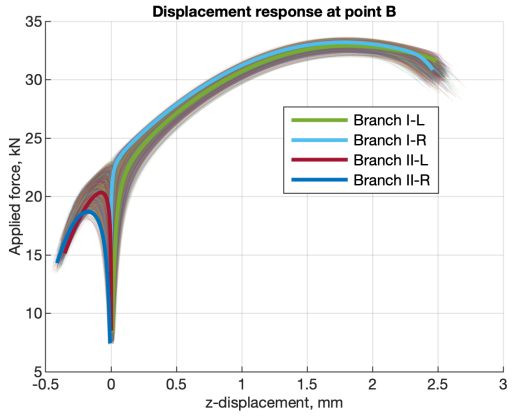

(b) Results of z-displacements at point B

Figure 5: z-displacement results of stochastic runs at points A and B shown in fig. 2, highlighting runs following different equilibrium branches

cal variations and the buckling load found, as discussed in section 2.3. Doing these calculations leads to the patterns found in fig. 7. Such patterns indicate the relative influence fiber angle variations have on the buckling load achieved. Patterns are continuous because variations are coupled to local distances through a correlation function, as discussed in section 2.2.2 and [28].

Applying the correlation function to the structure, changing the predefined fiber paths is done by scaling the fields, as discussed in section 2.3.2. Changing the scaling parameter m (eq. (20)) affects how the pattern applies to the fiber paths. Figures 9 to 11 shows examples with a scaling parameter m of 0.1, 1, and 10. Extreme scaling parameters used show how the pattern changes as the scaling parameter changes. Lower values for scaling parameter m lead to very aggressive fiber variations, with stronger curvatures in the path. Using high values leads to very local changes of orientation changes, retaining the original path in most of the structure. Scaling parameters close to 1 lead to a very smooth continuous fiber path without any quick changes.

A series of deterministic analyses are performed using a range of 1-20° maximum fiber variation ϕ, with a logarithmically spaced range of 21 different values between 0.1 and 10 for the scaling parameter m. Figure 8 shows these deterministic analyses' results, comparing the buckling load achieved with that of the baseline analysis done in section 3.2. Results show that the most significant deterministic improvement is achieved using small local changes in the fiber path. Using a maximum variation of 1°, a scaling parameter of $m = 10$ led to the largest increase in the buckling load by 51.1%. Such a small deviation is enough to nudge the structure into the stable branch II path shown in fig. 3a, which has a higher buckling load. As the fiber path perturbation increases in magnitude, the stiffness in the load-direction decreases, which reduces the buckling load, even when post-buckling branch II is triggered.

3.5. Robustness analysis

Stochastic results of section 3.3 shows that the equilibrium path of the baseline structure can switch due to localized fiber variations. Variation also exists within these equilibrium branches, in which these variations can positively or negatively influence the load achieved before instability occurs.

Robustness, in the context of this paper, refers to the influence such variations have on a structure. Quantitatively, this entails reducing the spread of the buckling load, ensuring that the stable equilibrium branch is followed while simultaneously reducing the standard deviation of the response.

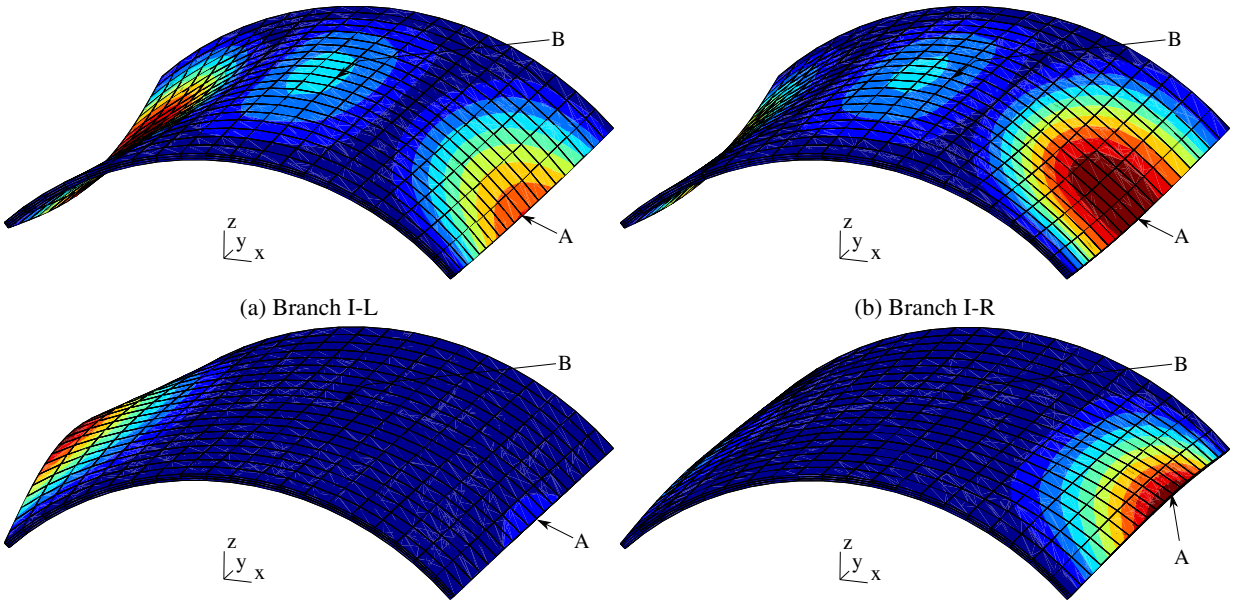

(a) Branch I-L (b) Branch I-R

(c) Branch II-L (d) Branch II-R

Figure 6: Scaled deformation shapes just past the buckling load, color indicates total relative deformation

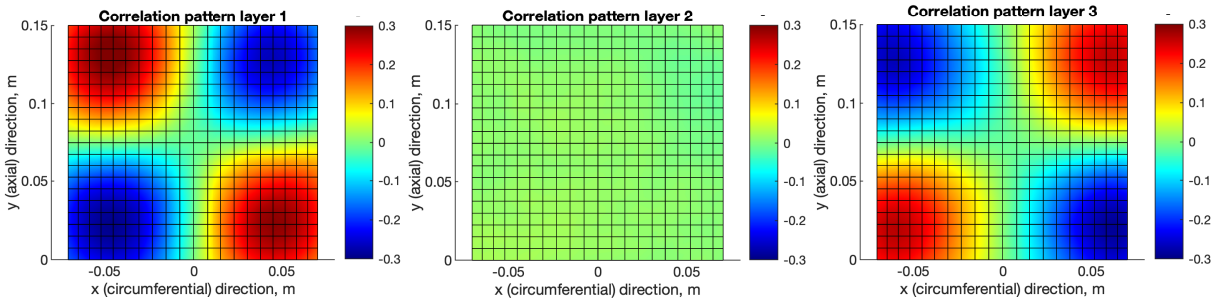

(a) Correlation pattern on the outer radius (b) Correlation pattern in the center layer (c) Correlation pattern on the inner radius

Figure 7: Correlation of local fiber angle variations and buckling load achieved

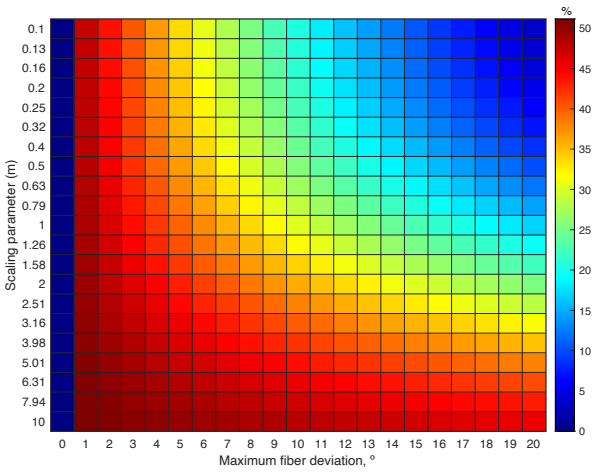

Figure 8: Percent increase in buckling load in deterministic results achieved by applying correlation patterns using eq. (20)

Stochastic analyses were performed on a selection of the configurations analyzed in section 3.3. Each configuration had 1000 samples computed, in which random fiber angle variations were applied. Variations were generated using the same parameters used in section 3.3, with $\sigma = 2°$ and a correlation length $L_c = 25$ mm.

Results indicate that the mean values shown in fig. 12 of specific configurations differ substantially from the deterministic results of section 3.4. Comparing the graph with that of the coefficient of variation in fig. 13, it is clear that this is due to different equilibrium paths being followed in specific configurations.

Figure 14 shows results of the structure with a maximum fiber variation of 2°, and a scaling factor of $m = 10$. 56% of the samples follow the stable path, with 44% following the unstable path followed in the baseline configuration. Compared to the 38% of the baseline structure, this is an improvement but still shows a significant unpredictability.

Seeking an optimal series of parameters of imperfect structures requires a reliability target under stochastic inputs. If, for example, the buckling load for 99% of the structures should exceed a target value, the statistical properties of the lower 1% can be analyzed. For the inputs given, the 1% values of the configurations are shown in fig. 15. Values are generated using either a fit Gaussian distribution (fig. 15a) or taking the lowest 1% of samples computed (fig. 15b). Configurations that consistently stay within one branch will show similar results in both of these figures. Configurations that follow both equilibrium paths will not fit Gaussian distributions. Comparing these figures shows which configurations are sensitive to branch jumping with the set variation and which are not.

Several configurations show similar performance. The ideal setup might, therefore, be related to manufacturing-related considerations. For example, the configuration with a maximum fiber variation of 8° and a scaling parameter of $m = 6.31$, with the fiber paths shown in fig. 17 has the distribution shown in fig. 16. Samples generated using those parameters follow the stable equilibrium path, 99.7% of all runs. Increasing the likelihood that the more stable branch II is followed significantly decreases the variability in the post-buckling response. Decreasing the variance while increasing the expectant value of the response of a structure makes the structure more robust while also increasing reliability [46].

4. Conclusion

Random fields make it possible to simulate the effects of local variations of fiber angles. The probability of an achieved design load despite imperfect fiber paths can be quantified. Structures with asymmetric post-buckling behavior, in which stable and unstable equilibria exist, can also be simulated. Fiber paths can directly influence the equilibrium path taken by introducing anisotropic behavior through, e.g., bend-twist coupling.

Processing on many samples with random local variations can map the local correlation to achieved load. Utilizing such a pattern to perturb the uniform fiber paths can improve the deterministic behavior of a structure by promoting a more stable post-buckling path.

Solutions offering the greatest deterministic improvement are often very sensitive to fiber misalignments. Structures such as those shown in the example might have two distinct equilibrium paths. Small perturbations can nudge an ideal structure towards the desired path but still leave it susceptible to random variations.

Combining perturbed structures with random variations makes it possible to quantify the chance that the desired equilibrium path is followed. Using statistical analysis on such combined runs makes it is possible to compute the minimum load achieved for a specific configuration. Parameters used to scale the field are a trade-off between mean improvement in the buckling load and the robustness of the structure, defined by likelihood to follow the more stable post-buckling path in the presence of fiber misalignments

Improvements found in the numerical example show increases in the order of 50%. The magnitude of improvement varies a lot by the specific structure analyzed

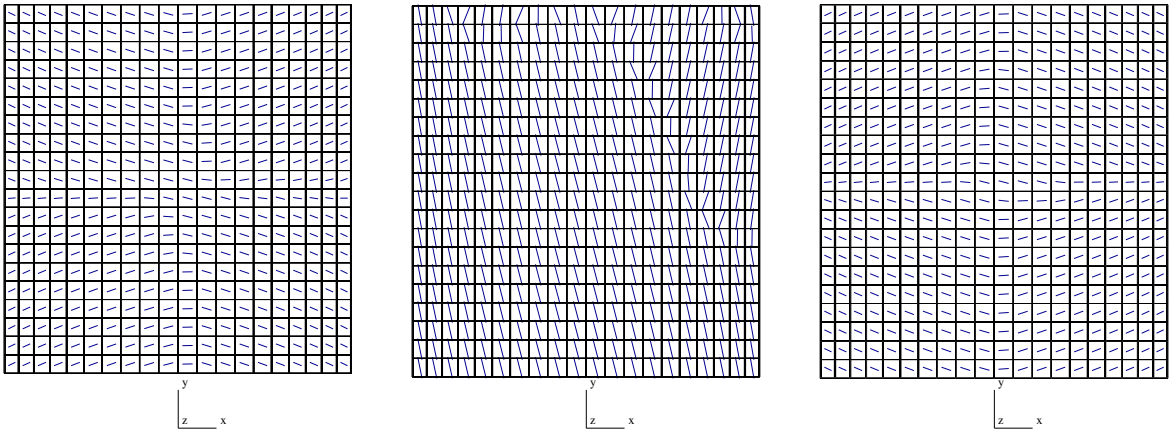

(a) Outer radius layer (b) Center layer (c) Inner radius layer

Figure 9: Fiber orientation for configuration with maximum variation of $\phi = 20°$ and scaling factor $m = 0.1$

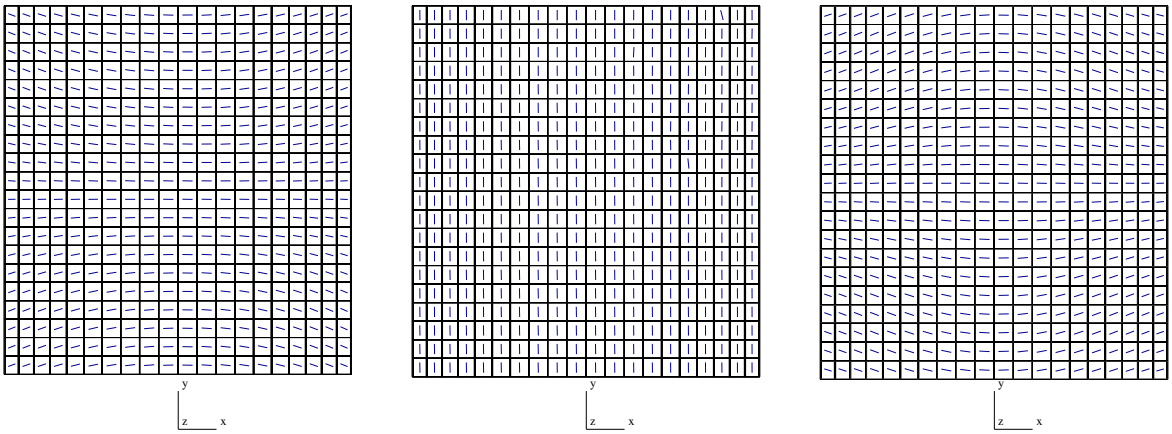

(a) Outer radius layer (b) Center layer (c) Inner radius layer

Figure 10: Fiber orientation for configuration with maximum variation of $\phi = 20°$ and scaling factor $m = 1$

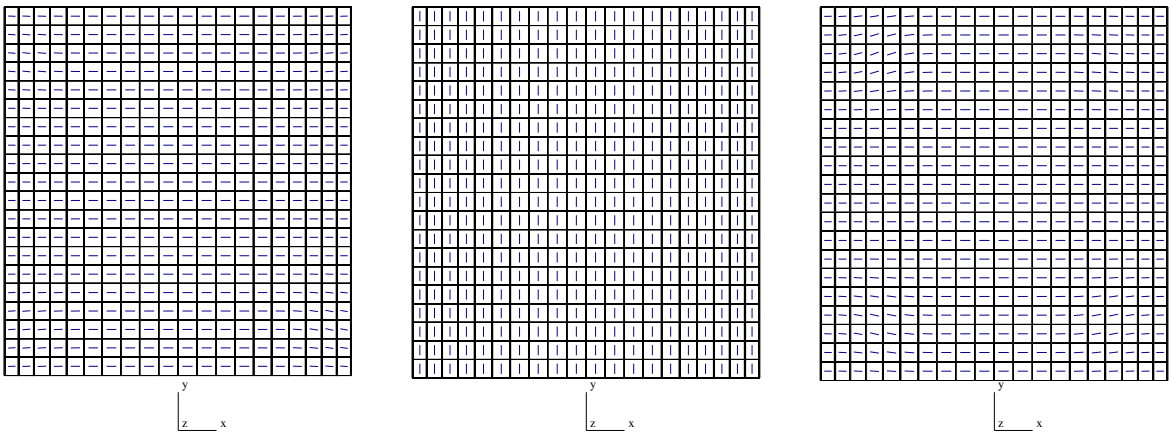

(a) Outer radius layer (b) Center layer (c) Inner radius layer

Figure 11: Fiber orientation for configuration with maximum variation of $\phi = 20°$ and scaling factor $m = 10$

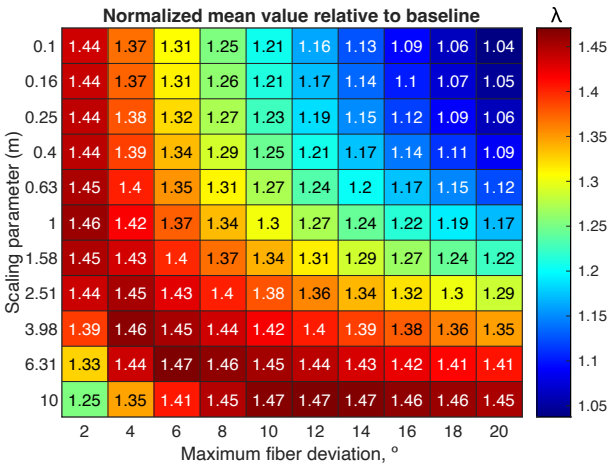

Figure 12: Mean value of buckling load for configurations with fiber angle variations of $\theta_\sigma = 2$ ° with $L_c = 25$ mm applied

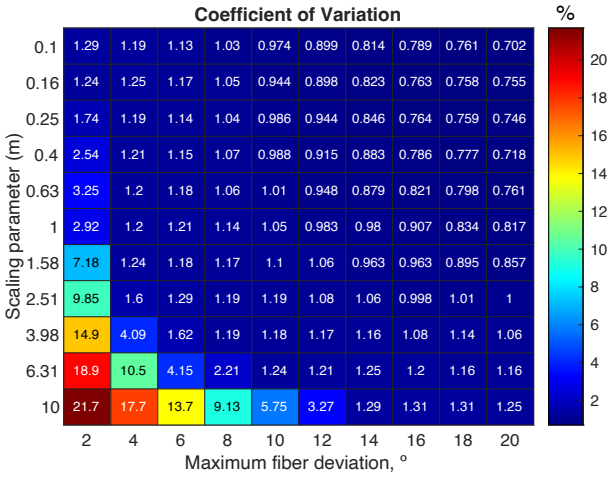

Figure 13: Coefficient of variation of configurations with fiber angle variations of $\theta_\sigma = 2$ ° with $L_c = 25$ mm applied

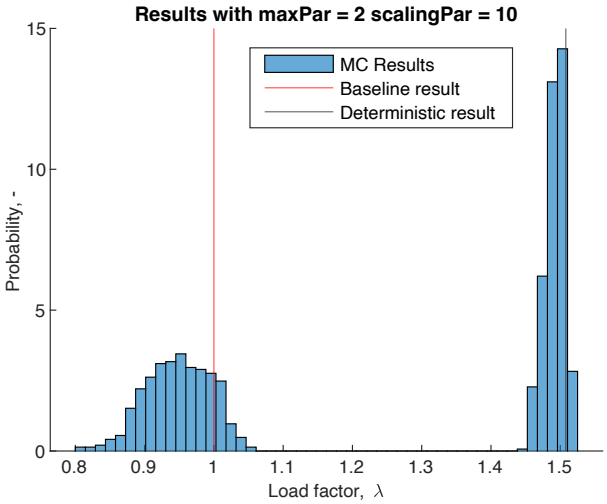

Figure 14: Probability density of samples with perturbed fiber paths with a maximum variation of $\phi = 2°$ and scaling parameter $m = 10$

and which equilibrium paths exist. Improvements can be higher than those of the example or lower. Improvements will also exist for other structures without a more stable post-buckling path nearby but will not be as significant. Instead of nudging the post-buckling path, the approach will redistribute the stiffnesses of a structure to increase the buckling load. Robustness, quantified by a reduction in variance, should be present in most structures.

Analyses presented in this work focus solely on fiber angle variations. Imperfections are not limited to such variations, and future work should take others, such as geometric, into account. No limits are present in the approach itself, as similar approaches have already been used for thickness and Young's modulus tailoring [28]. Combining multiple sources of variations can potentially further improve the insensitivity, and deterministic improvements presented.

Acknowledgements

This research work has been carried out within the project FULLCOMP (FULLy integrated analysis, design, manufacturing and health-monitoring of COMPosite structures), funded by the European Union Horizon 2020 Research and Innovation program under the Marie SkÅodowska-Curie grant agreement No. 642121.

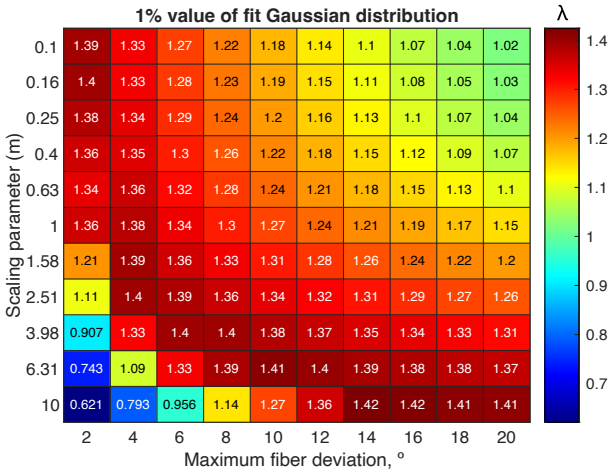

(a) 1% values of configurations obtained using Gaussian fit over numerical results

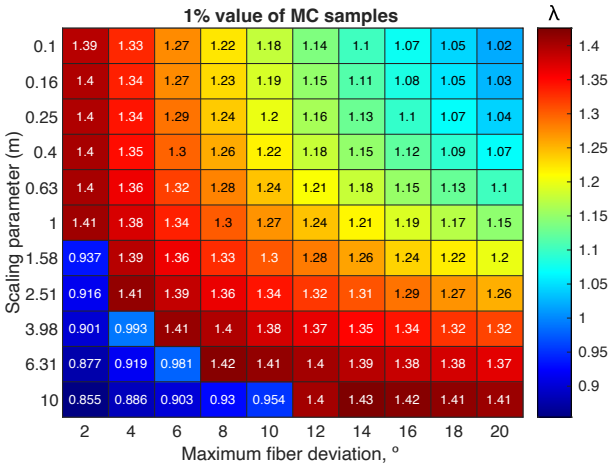

(b) 1% values of configurations obtained numerically

Figure 15: Lowest 1% values for the normalized buckling load for configurations with scaling parameters m and maximum fiber deviations ϕ applied according to eq. (20)

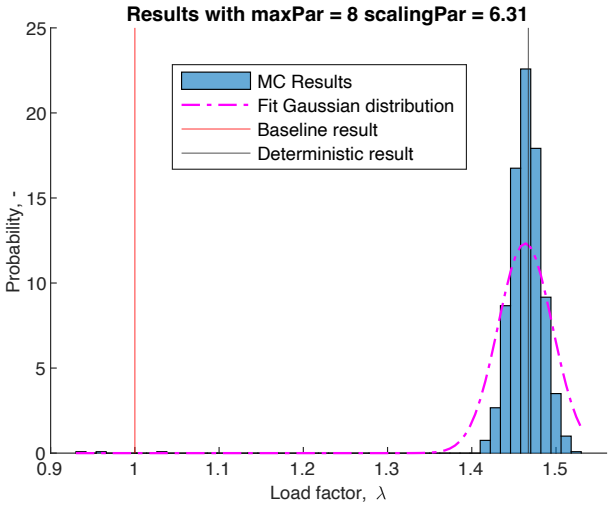

Figure 16: Probability density of samples with perturbed fiber paths with a maximum variation ϕ=8° and scaling parameter m = 6.31

The calculations presented here were partially carried out on the computing cluster system of the Leibniz University of Hannover, Germany.

Data availability

The raw data required to reproduce these findings may be made available on request

[1] C. R. Calladine, Understanding imperfection-sensitivity in the buckling of thin-walled shells, Thin-Walled Structures 23 (1995) 215–235.

[2] J. Kepple, M. T. Herath, G. Pearce, B. Gangadhara Prusty, R. Thomson, R. Degenhardt, Stochastic analysis of imperfection sensitive unstiffened composite cylinders using realistic imperfection models, Composite Structures 126 (2015) 159–173.

[3] A. Manta, M. Gresil, C. Soutis, Infrared thermography for void mapping of a graphene/epoxy composite and its full-field thermal simulation, Fatigue and Fracture of Engineering Materials and Structures (2019) 1–13.

[4] S. W. Yurgartis, Measurement of small angle fiber misalignments in continuous fiber composites, Composites Science and Technology 30 (1987) 279–293.

[5] P. Sasikumar, R. Suresh, P. K. Vijayaghosh, S. Gupta, Experimental characterisation of random field models for CFRP composite panels, Composite Structures 120 (2015) 451–471.

[6] S. Sriramula, M. K. Chryssanthopoulos, An experimental characterisation of spatial variability in GFRP composite panels, Structural Safety 42 (2013) 1–11.

[7] T. J. Dodwell, S. Kinston, R. Butler, R. T. Haftka, N. H. Kim, R. Scheichl, Multilevel Monte Carlo Simulations of Composite Structures with Uncertain Manufacturing Defects, 2019.

[8] G. Stefanou, D. Savvas, M. Papadrakakis, Stochastic finite element analysis of composite structures based on mesoscale random fields of material properties, Computer Methods in Applied Mechanics and Engineering 326 (2017) 319–337.

[9] C. Scarth, S. Adhikari, P. H. Cabral, G. H. C. Silva, A. P. d. Prado, P. Higino, G. H. C. Silva, A. P. d. Prado, Random field simulation over curved surfaces : Applications to computational

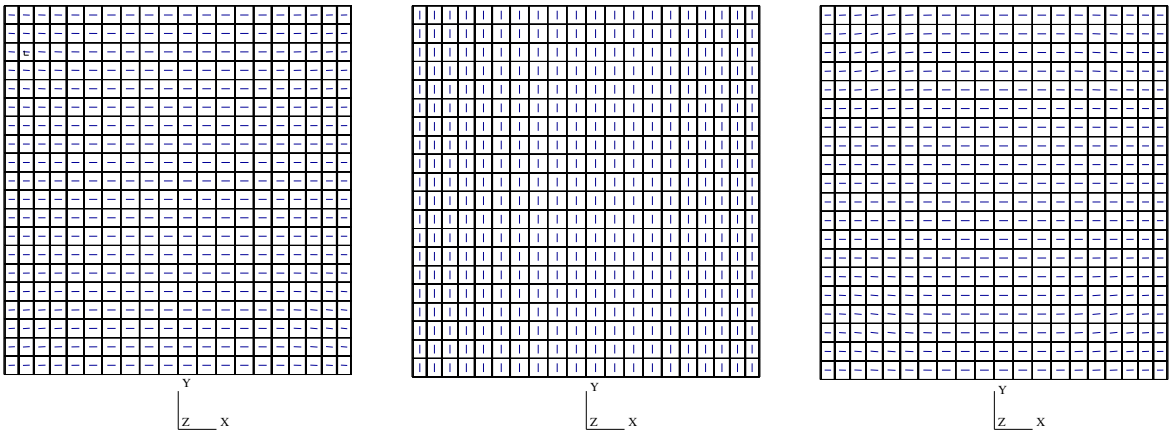

(a) Outer radius layer (b) Center layer (c) Inner radius layer

Figure 17: Fiber orientation for configuration with maximum variation of $\phi = 8^\circ$ and scaling factor $m = 6.31$

structural mechanics, Computer Methods in Applied Mechanics and Engineering 345 (2019) 283–301.

[10] S. v. d. Broek, E. Jansen, S. Minera, P. M. Weaver, R. Rolfes, Effect of spatially varying material properties on the post-buckling behaviour of composite panels utilising geodesic stochastic fields, in: Proceedings of the 6th Aircraft Structural Design conference, Bristol, United Kingdom.

[11] V. Papadopoulos, M. Papadrakakis, The effect of material and thickness variability on the buckling load of shells with random initial imperfections, Computer Methods in Applied Mechanics and Engineering 194 (2005) 1405–1426.

[12] M. Tootkaboni, L. Graham-Brady, B. W. Schafer, Geometrically non-linear behavior of structural systems with random material property: An asymptotic spectral stochastic approach, Computer Methods in Applied Mechanics and Engineering 198 (2009) 3173–3185.

[13] N. Hu, R. Burgueño, Cylindrical Shells with Tunable Post-buckling Features Through Non-Uniform Patterned Thickening Patches, International Journal of Structural Stability and Dynamics 18 (2018) 1850026.

[14] N. Hu, R. Burgueño, Harnessing Seeded Geometric Imperfection to Design Cylindrical Shells With Tunable Elastic Post-buckling Behavior, Journal of Applied Mechanics 84 (2017) 011003.

[15] B. S. Cox, R. M. Groh, D. Avitabile, A. Pirrera, Modal nudging in nonlinear elasticity: Tailoring the elastic post-buckling behaviour of engineering structures, Journal of the Mechanics and Physics of Solids 116 (2018) 135–149.

[16] B. S. Cox, R. M. Groh, A. Pirrera, Nudging Axially Compressed Cylindrical Panels Toward Imperfection Insensitivity, Journal of Applied Mechanics, Transactions ASME 86 (2019).

[17] M. W. Hyer, R. F. Charette, Use of curvilinear fiber format in composite structure design, AIAA Journal 29 (1991) 1011–1015.

[18] Z. Gürdal, B. F. Tatting, C. K. Wu, Variable stiffness composite panels: Effects of stiffness variation on the in-plane and buckling response, Composites Part A: Applied Science and Manufacturing 39 (2008) 911–922.

[19] Z. Wu, G. Raju, P. M. Weaver, Postbuckling analysis of variable angle tow composite plates, International Journal of Solids and Structures 50 (2013) 1770–1780.

[20] B. H. Coburn, Z. Wu, P. M. Weaver, Buckling analysis of stiffened variable angle tow panels, Composite Structures 111 (2014) 259–270.

[21] A. Haldar, R. M. Groh, E. Jansen, P. M. Weaver, R. Rolfes, An efficient semi-analytical framework to tailor snap-through loads in bistable variable stiffness laminates, International Journal of Solids and Structures 195 (2020) 91–107.

[22] A. W. Blom, C. S. Lopes, P. J. Kromwijk, Z. Gürdal, P. P. Camanho, A theoretical model to study the influence of tow-drop areas on the stiffness and strength of variable-stiffness laminates, Journal of Composite Materials 43 (2009) 403–425.

[23] M. Rakhshbahar, M. Sinapius, A Novel Approach: Combination of Automated Fiber Placement (AFP) and Additive Layer Manufacturing (ALM), Journal of Composites Science 2 (2018) 42.

[24] B. C. Kim, K. Potter, P. M. Weaver, Continuous tow shearing for manufacturing variable angle tow composites, Composites Part A: Applied Science and Manufacturing 43 (2012) 1347–1356.

[25] T. J. Dodwell, R. Butler, A. T. Rhead, Optimum fiber steering of composite plates for buckling and manufacturability, AIAA Journal 54 (2016) 1139–1142.

[26] J. Marczyk, Stochastic multidisciplinary improvement - Beyond optimization, 8th Symposium on Multidisciplinary Analysis and Optimization (2000).

[27] S. C. White, G. Raju, P. M. Weaver, Initial post-buckling of variable-stiffness curved panels, Journal of the Mechanics and Physics of Solids 71 (2014) 132–155.

[28] S. van den Broek, S. Minera, A. Pirrera, P. M. Weaver, E. Jansen, R. Rolfes, Enhanced deterministic performance of panels using stochastic variations of geometry and material, AIAA Journal 58 (2020) 2307–2320.

[29] S. Minera, M. Patni, E. Carrera, M. Petrolo, P. M. Weaver, A. Pirrera, Three-dimensional stress analysis for beam-like structures using Serendipity Lagrange shape functions, International Journal of Solids and Structures 141-142 (2018) 279–296.

[30] M. Patni, S. Minera, P. M. Weaver, A. Pirrera, Efficient modelling of beam-like structures with general non-prismatic, curved geometry, Computers and Structures 240 (2020) 106339.

[31] R. d. Borst, M. A. Crisfield, J. J. C. Remmers, C. V. Verhoosel, Non-Linear Finite Element Analysis of Solids and Structures, Wiley, Sussex, United Kingdom, 2012.

[32] A. Pagani, E. Carrera, Unified formulation of geometrically nonlinear refined beam theories, Mechanics of Advanced Mate-

rials and Structures 25 (2018) 15–31.
[33] S. Minera, Analysis and Design of Buckling Resistant Thin-Walled Structures via Computationally Efficient 3D Stress Analysis, Ph.D. thesis, University of Bristol, 2019.
[34] M. Patni, S. Minera, C. Bisagni, P. Weaver, A. Pirrera, Geometrically nonlinear finite element model for predicting failure in composite structures, Composite Structures 225 (2019) 111068.
[35] E. W. Dijkstra, A note on two problems in connexion with graphs, Numerische Mathematik 1 (1959) 269–271.
[36] P. Bose, A. Maheshwari, C. Shu, S. Wuhrer, A survey of geodesic paths on 3D surfaces, Computational Geometry: Theory and Applications 44 (2011) 486–498.
[37] S. R. S. Varadhan, On the behavior of the fundamental solution of the heat equation with variable coefficients, Communications on Pure and Applied Mathematics 20 (1967) 431–455.
[38] K. Crane, C. Weischedel, M. Wardetzky, The Heat Method for Distance Computation, Communications of the ACM 60 (2017) 90–99.
[39] P. D. Spanos, B. A. Zeldin, Monte Carlo Treatment of Random Fields: A Broad Perspective, Applied Mechanics Reviews 51 (1998) 219.
[40] F. M. Dekking, C. Kraaikamp, H. P. Lopuhaä, L. E. Meester, A Modern Introduction to Probability and Statistics: Understanding why and how, Springer Science & Business Media, 2005.
[41] A. Pagani, A. R. Sanchez-Majano, Stochastic stress analysis and failure onset of variable angle tow laminates affected by spatial fibre variations, Composites Part C: Open Access 4 (2021) 100091.
[42] A. Pagani, A. R. Sanchez-Majano, Influence of fiber misalignments on buckling performance of variable stiffness composites using layerwise models and random fields, Mechanics of Advanced Materials and Structures 0 (2020) 1–15.
[43] K. Sepahvand, Spectral stochastic finite element vibration analysis of fiber-reinforced composites with random fiber orientation, Composite Structures 145 (2016) 119–128.
[44] M. W. Davis, Production of conditional simulations via the LU triangular decomposition of the covariance matrix, Mathematical Geology 19 (1987) 91–98.
[45] C.-C. Li, A. Der Kiureghian, Optimal discretization of random fields, Journal of engineering mechanics 119 (1993) 1136–1154.
[46] W. Yao, X. Chen, W. Luo, M. Van Tooren, J. Guo, Review of uncertainty-based multidisciplinary design optimization methods for aerospace vehicles, Progress in Aerospace Sciences 47 (2011) 450–479.
[47] E. J. Barbero, Introduction to Composite Materials Design, CRC Press, 2nd editio edition, 2011.